Spring 2015

# Developing a novel methodolgy and testbed for fatigue analysis of metal specimens

Sai Aravind Palepu



Department:

# DEVELOPING A NOVEL METHODOLGY AND TESTBED FOR FATIGUE ANALYSIS OF METAL SPECIMENS

by

SAI ARAVIND PALEPU

A THESIS

Presented to the Faculty of the Graduate School of the

MISSOURI UNIVERSITY OF SCIENCE AND TECHNOLOGY

In Partial Fulfillment of the Requirements for the Degree

MASTER OF SCIENCE IN MANUFACTURING ENGINEERING

2015

Approved by

Dr. Frank Liou, Advisor
Dr. Edward C. Kinzel
Dr. Heng Pan

## ABSTRACT

A prototype of fatigue testing machine was built to determine the fatigue strength of materials. Proposed testing prototype was displacement controlled magnetic type bend fatigue testing machine. Designed prototype was tuned to operate at or near resonance of the specimen in order to amplify excitation displacement. Low maintenance i.e. zero wear of the parts was achieved, there were no moving components in the prototype machine. Crucial components used to build were: DC power supply, solenoid, Arduino UNO, supports and laser displacement sensor. DC source used to pass current through solenoid producing magnetic field; mosfet and Arduino generated square waves of the magnetic field; supports held the specimen as simple-simple supports close to the solenoid; and laser displacement sensor recorded the displacements of the specimen. Using Euler-Bernoulli beam theory, for a simple-simple supported beam the strain was calculated from the radius of curvature of the bent beam. Using the built prototype, Aluminum 6061-T6 was tested at different strains and its respective cycles to failure was recorded. The S-N curve for Aluminum 6061-T6 obtained experimentally using prototype fatigue testing machine was compared to ASTM results.

# ACKNOWLEDGMENTS

The current work presented was supported and encouraged by following people. The exposure and experience I gained during my stay at Missouri S&T is invaluable and I am thankful to Dr. Frank Liou for his guidance and encouragement without which all this would not have happened. I am immensely grateful to Dr. Frank Liou for giving me an opportunity to work at LAMP lab. I am thankful to Todd E Sparks for his encouragement, advice and patience throughout my work. The insight and suggestions provided by Max and Benjamin were helpful for successful completion of the project. I must also thank Manufacturing Engineering Program for the financial assistance provided. I would like to thank Missouri S&T Mechanical Engineering machine shop and Material Research Center for their valuable contribution and support to the project.

I would like to thank Dr. Edward Kinzel for the close participation, advice and guidance that he has provided throughout the journey. I would also like to thank Dr. Heng Pan for his time and advice provided during this research. I would like to thank them for being a part of my thesis committee.

I most sincerely thank the members of the LAMP lab for making this journey educational and exciting. I would specially like to thank Sreekar Karnati, Niroop Matta and Praneeth Isanaka for their assistance and critique throughout this journey. I am also grateful to Vivek Thotla, PhaniKrishna Kalakonda and 101-19 group for their support and memories during my stay.

Finally, I would like to express my deep gratitude to my parents, Jagannadh Palepu and Sreedevi Palepu, and my dear brother Abhiram Palepu for their unconditional love and support.

# TABLE OF CONTENTS

# LIST OF ILLUSTRATIONS

# LIST OF TABLES

# 1. INTRODUCTION

## 1.1. LITERATURE REVIEW

Structure having one of its dimensions much larger than the other two is called a beam. The axis of the beam is defined along that longer dimension, and a cross section normal to this axis is assumed to smoothly vary along the span or length of the beam. The structural analysis for beams can be performed with various beam theories. One of the simplest and most useful of these theories was Euler- Bernoulli beam theory [1]. A fundamental assumption of this theory is that the cross section of the beam is infinitely rigid in its own plane, *i.e.*, no deformations occur in the plane of the cross-section. Consequently, the in-plane displacement field can be represented simply by two rigid body translations and one rigid body rotation. This fundamental assumption deals only with in-plane displacements of the cross-section. Two additional assumptions deal with the out-of-plane displacements of the section: during deformation, the cross-section is assumed to remain plane and normal to the deformed axis of the beam.

Euler-Bernoulli equation describes the relationship between the beams deflection and the applied load. The dynamic beam equation is the Euler-Lagrange equation:

$$EI\left(\frac{\partial^4 y}{\partial x^4}\right) + \mu\left(\frac{\partial^2 y}{\partial t^2}\right) = F(t) \qquad (1)$$

First term in the equation (1) the potential energy due to internal forces where E is the Youngs modulus and I is the second moment of area; the second term represents kinetic energy where $\mu$ is the mass per unit length and the third term represents the potential energy due to the external load F(t). From Euler-Bernoulli beam theory solution for simple-simple supported beams, the frequency of the beam and strain is determined.

Structures may not show significant (perceptible) effect at calculated (steady static) loads, but repeated loading on the structure may have significant effect. These failures were termed as fatigue failure. The broken part shows, usually at the surface, a spot or nucleus at which, after many cycles of stress, a crack started and then progressed gradually during some additional thousands of cycles, until the piece was nearly cracked through. As the crack propagates, the cross sectional area will be too small to take one more stress cycle, and a brittle fractures occurs [2].

Generally fatigue tests are conducted to evaluate the endurance limit of the material. Endurance limit is defined as the cyclic stress which can run certain number of cycles without fatigue failure and this limit varies with the purpose/usage of material. Materials like titanium and ferrous metals have an endurance limit, S-N curve for these materials will not go to infinity i.e. the material will never fail below endurance limit. And S-N curve for few materials like aluminum and certain steel alloys will touch the abscissa i.e. they will fail at low stresses for very large number of cycles ($10^8$ or more). For these materials, like aluminum, the endurance limit will be defined as the stress that can survive $10^6$ or $10^7$ cycles, usually 40 percent of material's yield strength ($10^6$ cycles). After conducting tests on materials, the selected endurance limit was then calculated my multiplying correcting factors to get true endurance limit. The major factors that greatly influence the endurance limit were size, shape, surface finish, loading, temperature etc.

The presented study experimentally researches the concept of fatigue testing a beam using magnetic impulses to induce repeated bending stresses at near resonant frequencies of the specimen. Mechanically driven repeated bending fatigue machines were commercially available with 20,000 lb. capacity and speeds up to 1750 rpm [3] and simple oscillator form of magnetic machine using electromagnetism producing vibrations from 1200 to 600,000 cycles per minute [4]. However, electro-magnetically excited machines generally have low testing forces than mechanically driven machines. The principle of electromagnetism says that a current carrying conductor produces magnetic field, when current flows through tightly coiled conducting wire a strong magnetic field is created and the coil acts like a magnet. The polarity depends on the direction of flow of current through the coil. There are few designs of fatigue testing machines, which use this magnetism principle. The Rayflex machine uses AC current continuously changing the polarity, this will help in pulling and pushing the cantilever specimen. Magnetic-type machines produce periodical disturbing force generally used to cause forced vibrations of the system containing the test specimen. This system is usually tuned to operate at or near resonance of the disturbing force in to amplify excitation force. Usually magnetic type fatigue testing machines apply low loads but work at high speeds.

Proposed design of the fatigue machine works on DC power supply, no change in polarity of the solenoid. The principle of resonance was applied in this design, consider a rubber mallet striking tuning fork, as the rate of strikes reaches the natural frequency of the fork, the amplitude of vibration on the tuning fork increases. Similarly to the mallet striking rate, a small pulse of current was flown through the solenoid and this pulse is converted to magnetic pulse by the coil. During this small pulses, the solenoid has it polarity constant everytime. A small permanent magnet was glued at the midsection of the specimen length and placed near the coil end in a way that the face of the magnet towards the coil should have same polarity. This setup initially attracted the specimen when there was no current flow, because of the ferritic core rod used in solenoid. As the test begins, the current passing through the solenoid generates magnetic field and the solenoid acts as a magnet with poles. The poles of the temporary solenoid magnet depends on the direction of flow of current. The face of the solenoid and the permanent magnet glued to specimen was arranged to have like poles, as like poles repel, the short duration of pulse will strike the specimen away. As the current flow stops, the ferrite rod and the magnet on specimen will be attracted. Specimen vibrates and bends at the center inducing strain cyclically as shown in figure 1.1. Establishing following theory to calculate the stresses, solenoid design and support design is crucial to perform a fatigue failure test on any material.

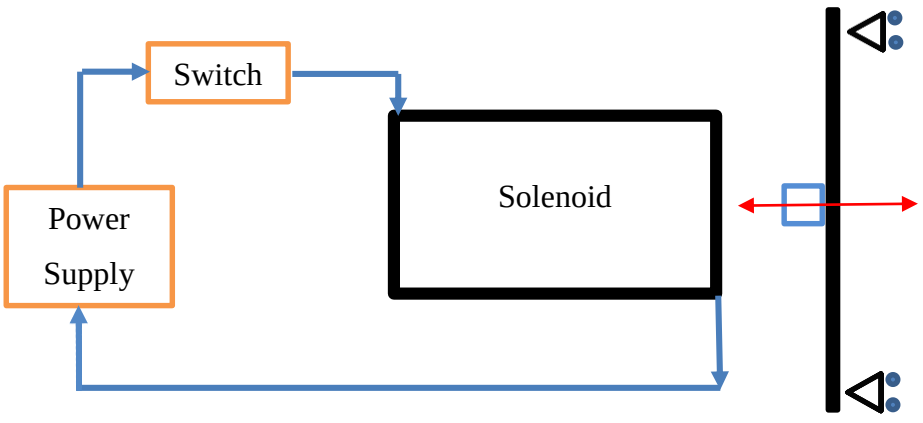


Figure 1.1 General representation of the test setup

## 1.2. THEORY

Euler-Lagrange equation (1) is solved in the following equations. Separating two dependent variables spatial Y(x) and time T(t) and considering F(t) = 0

$$y(x,t) = Y(x) \times T(t) \tag{2}$$

$$EI\left(\frac{\partial^4 Y(x)T(t)}{\partial x^4}\right) + \mu\left(\frac{\partial^2 Y(x)T(t)}{\partial t^2}\right) = 0 \tag{3}$$

$$EI\,T(t)\left(\frac{\partial^4 Y(x)}{\partial^4 x}\right) = -\mu\,Y(x)\left(\frac{\partial^2 T(t)}{\partial^2 t}\right) \tag{4}$$

$$\frac{E\,I}{\mu}\,\frac{\left(\frac{\partial^4 Y(x)}{\partial x^4}\right)}{Y(x)} = -\,\frac{\left(\frac{\partial^2 T(t)}{\partial t^2}\right)}{T(t)} = \omega^2 \tag{5}$$

Spatial term, Y(x) is the mode shape function determined from the eigenvalue & Eigen function analysis [5], [6].

$$\frac{E\,I}{\mu}\left(\frac{\partial^4 Y(x)}{\partial x^4}\right) = Y(x)\,\omega^2 \tag{6}$$

$$\frac{E\,I}{\mu}\,\frac{\left(\frac{\partial^4 Y(x)}{\partial x^4}\right)}{Y(x)} = \omega^2 \tag{7}$$

$$\left(\frac{\partial^4 Y(x)}{\partial x^4}\right) = \beta^4 Y(x) \tag{8}$$

$$\beta^4 = \frac{\mu}{E\,I}\omega^2 \tag{9}$$

General solution to equation (8) is,

$$Y(x) = a_1\sinh(\beta x) + a_2\cosh(\beta x) + a_3\sin(\beta x) + a_4\cos(\beta x) \tag{10}$$

The values of constants $a_1$, $a_2$, $a_3$ and $a_4$ are solved using boundary conditions. For Simply Supported Beam, deflection and moment at the pinned ends are zero. Table 1.1 shows the conditions, applies and solves equation (10).

Table 1.1 Boundary conditions for simple-simple support beam

| Condition- 1 | Condition- 2 |
|---|---|
| At x=0<br>Deflection=0 i.e. Y(x)=0<br>Moment=0 i.e. $d^2$ Y(x) / $dx^2$=0 | At x=L<br>Deflection=0 i.e. Y(x)=0<br>Moment=0 i.e. $d^2$ Y(x) / $dx^2$=0 |
| $a_2 + a_4$=0<br>$a_2 - a_4$=0<br>$a_2 = a_4$=0 | $a_1\sinh(\beta L) + a_3\sin(\beta L)$=0<br>$a_1\sinh(\beta L) - a_3\sin(\beta L)$=0<br>$a_1$ = 0 |

Applying boundary conditions, the values of $a_2$ and $a_4$ are calculated to be zero. $a_1\sinh(\beta L)$ can be equal zero only if the $a_1$ value is zero and $a_3 \sin(\beta L) = 0$ can be satisfied only when $a_3$ not equal to zero. Hence, the solution for spatial variable is given in equation (11) and the first mode shape is shown in the Fig.1.2 where y-axis is the displacement and x-axis represents the length of the beam,

$$Y(x) = a_3 \sin(\beta x) \tag{11}$$

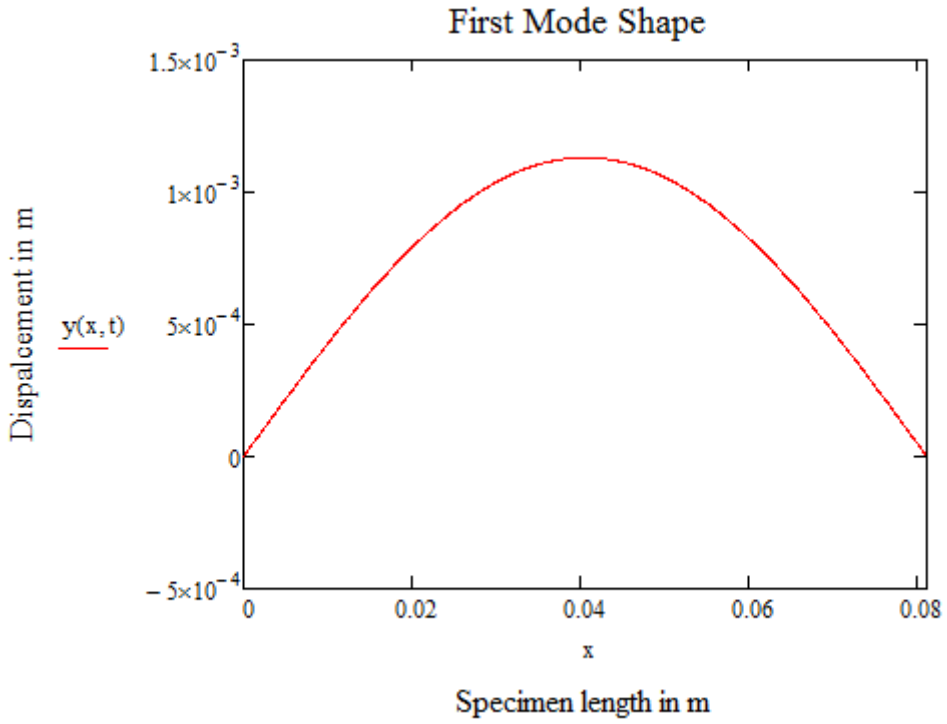


Figure 1.2 First mode shape over the length of the specimen

Using the above boundary condition: 2, β value can be determined from,

$$\begin{bmatrix} \sinh(\beta L) & \sin(\beta L) \\ \sinh(\beta L) & \sin(\beta L) \end{bmatrix} \begin{matrix} a_1 \\ a_3 \end{matrix} = \begin{matrix} 0 \\ 0 \end{matrix} \tag{12}$$

Solving the matrix gives the following solution

$$\sin(\beta L) \times \sinh(\beta L) = 0 \tag{13}$$

$$\beta \times L = n \times \pi \tag{14}$$

First mode (n=1) natural frequency of the specimen derived from the above equation (9) and equation (14) is given below [7], [8],

$$\omega = \left(\frac{n\times\pi}{L}\right)^2 \sqrt{\frac{E\,I}{\mu}} \tag{15}$$

Time variable, T(t) is the modal amplitude, Here impulse force $F_e$, is applied for average time interval of t. Constitutive equation for a beam with damping co efficient (c) and time dependent forcing function F(t)is given below,

$$EI\left(\frac{\partial^4 y}{\partial x^4}\right) + c\left(\frac{\partial y}{\partial t}\right) + \mu\left(\frac{\partial^2 y}{\partial t^2}\right) = F(t) \tag{16}$$

Now multiplying Y(x) spatial term, integrating with respect to x between 0 and L, and applying orthogonality conditions, we get,

$$EI\left(\frac{\partial^4 y}{\partial x^4}\right)\int_0^L Y(x) + c\left(\frac{\partial y}{\partial t}\right)\int_0^L Y(x) + \mu\left(\frac{\partial^2 y}{\partial t^2}\right)\int_0^L Y(x) = F(t)\int_0^L Y(x) \tag{17}$$

$$\frac{EI\,T(t)}{\mu}\left(\frac{\partial^4 Y(x)}{\partial x^4}\right)\int_0^L Y(x)^2 + \frac{c}{\mu}\left(\frac{\partial T(t)}{\partial t}\right)\int_0^L Y(x)^2 + \left(\frac{\partial^2 T(t)}{\partial t^2}\right)\int_0^L Y(x)^2 = F(t)\int_0^L Y(x) \tag{18}$$

$$\frac{EI\,\beta^4 T(t)}{\mu}\int_0^L Y(x)^2 + \frac{c}{\mu}\left(\frac{\partial T(t)}{\partial t}\right)\int_0^L Y(x)^2 + \left(\frac{\partial^2 T(t)}{\partial t^2}\right)\int_0^L Y(x)^2 = \frac{F(t)}{\mu}\int_0^L Y(x) \tag{19}$$

$$\int_0^L Y(x)^2 \times \mu = M_a \tag{20}$$

$M_a$is the modal mass and the damping ration $\xi$ is defined as,

$$\frac{c}{\mu} = 2 \times \omega \times \xi \tag{21}$$

$$\omega^2\, T(t) + \frac{c}{\mu}\left(\frac{\partial T(t)}{\partial t}\right) + \left(\frac{\partial^2 T(t)}{\partial t^2}\right) = \frac{F(t)}{M_a}\int_0^L Y(x) \tag{22}$$

Here F(t), a time dependent forcing function [9], is a large constant force applied on very small time interval i.e.

$$F(t) = \begin{cases} \frac{A}{\epsilon}, & if\ 0 < t < \epsilon \\ 0, & otherwise \end{cases} \tag{23}$$

$$\int_{-\infty}^{+\infty} F(t)dt = A \tag{24}$$

The value of A is unity, if F(t) is a unit impulse with units Newton seconds. Let $X_\epsilon(t)$ be the solution for the time variable equation, consider F(t) = $F_\epsilon(t)$ and then taking Laplace transform [10],

$$\mathcal{L}\{f_e(t)\} = \int_0^\infty e^{-st} f_e(t)\ dt = \frac{1-e^{-\epsilon s}}{\epsilon s} \tag{25}$$

For any s greater than zero, $\lim_{\epsilon \to 0} \frac{1-e^{-\epsilon s}}{\epsilon s} = 1$ (26)

Now applying Laplace transform to equation (22) considering initial conditions as $x^1(0) = x(0) = 0$

$$\omega^2\, X_\epsilon(s) + 2\omega\, s\, \xi X_\epsilon(s) + s^2 X_\epsilon(s) = \frac{\frac{1-e^{-\epsilon s}}{\epsilon s}}{M_a} \int_0^L \sin(\beta x)\, dx \tag{27}$$

As, $s \to 0$,

$$X_\epsilon(s) = \frac{a}{s^2 + 2\omega\, \xi\, s + \omega^2} \tag{28}$$

Let,

$$\frac{\frac{1-e^{-\epsilon s}}{\epsilon s}}{M_a} \int_0^L \sin(\beta x)\, dx = \frac{2}{\beta M_a} = a \tag{29}$$

As the roots for the quadratic polynomial equation $ax^2 + bx + c = 0$ with $a \neq 0$ is given by,

$$x = \frac{-b \pm \sqrt{b^2 - 4ac}}{2a}$$

Similarly solving the above equation, roots solved are,

$$r_1, r_2 = -\omega\, \xi \pm j\omega_d \tag{30}$$

Here, $\omega_d = \omega\sqrt{1-\xi^2}$ is the damped frequency and for under damped conditions, $\xi < 1$. Now, rearranging the above equation (28) with the solution derived,

$$X_\epsilon(s) = \frac{a}{(s + \omega\, \xi - j\omega_d)(s + \omega\, \xi + j\omega_d)} \tag{31}$$

Performing partial fraction decomposition to the equation, inverse Laplace transformation is applied to the decomposed equation (31),

$$X_\epsilon(t) = \frac{2}{\omega_d \beta M_a} e^{-\omega \xi t} \sin(\omega_d t) \tag{32}$$

Combining the two solutions, the final solution is derived. The final solution gives the displacement of a point on beam (x) at any given time (t).

$$y(x,t) = \frac{2\sin(\beta x)}{\omega_d \beta M_a} e^{-\omega \xi t} \sin(\omega_d t) \tag{33}$$

The solution derived from the governing equation was plotted using Mathcad, Fig.1.3 shows the dampening of specimen with time when a single impulse was given [11].

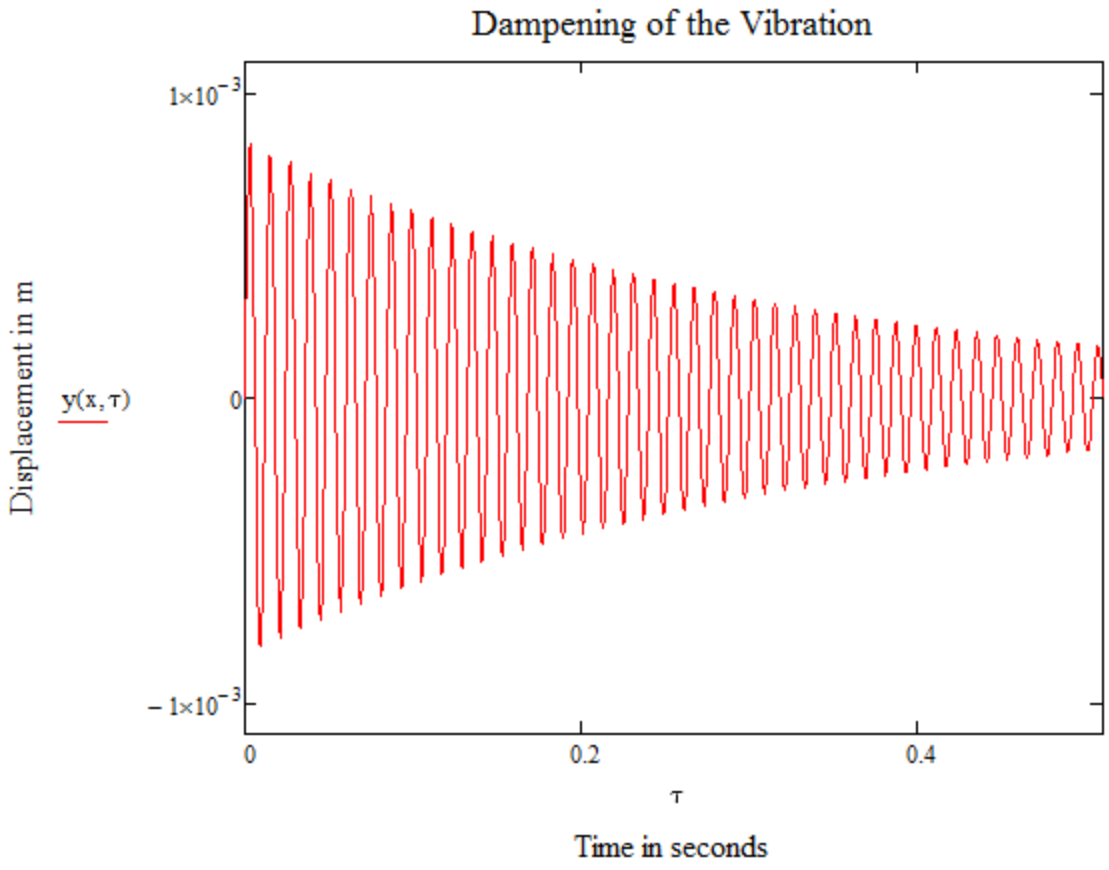


Figure 1.3 Displacement profile of midpoint of specimen with time for single impulse

From the displacement equation, radius of curvature can be calculated and related to strain with the mentioned equation.

$$\sigma = \frac{M \times Z}{I} \tag{34}$$

$$E \times \varepsilon = -Z \times E \times \frac{\partial^2 y}{\partial x^2} \tag{35}$$

$$Strain(\varepsilon) = -Z \times \frac{\partial^2 y}{\partial x^2} \tag{36}$$

Here, Z is the distance from the neutral axis of the beam and M is the bending moment. This equation is valid only for true bending i.e. zero stresses at the neutral axis.

Solenoid, the forcing component to bend the specimen, was designed considering electromagnetism [12]. Current passing through solenoid creates magnetic field, the strength of the field was mainly influenced by density of turns in the coil and the current flowing through it. The below expression shows the magnetic field strength B:

$$B = \frac{\mu_0 \times N \times I}{2}\left[\frac{D+L}{\sqrt{(D+L)^3+R^2}} - \frac{D}{\sqrt{D^2+R^2}}\right] \quad (37)$$

Where, $\mu_0$is magnetic permeability which is a constant, N is the number of turns in coil per meter, I is the current passing through coil, D is the distance from edge of the solenoid, L is the length of coiled wire and $R$ is the radius of coiled wire.

# 2. EXPERIMENTAL SETUP

## 2.1. DESIGN

The main aim of this study was to model a cost and time effective bend fatigue tester. An optimized specimen had to be designed to test on the built prototype machine. Conventional fatigue testing machines use cantilever specimen, tapered to the free end where the loads were applied. Repeated bending tests are largely used to investigate sheet and plate materials. Specimen was designed to occur failure at the analyzed zone and avoid failure at the grips or supports. All the theory were performed considering a flat thin rectangular specimen, but when experimentally tested, the specimen has always failed at the edge of the magnet as the stresses are high at the specimen center for simple supported beam. Figure 2.1 shows the failure of the 3D printed specimen at the edge of the glued magnet. After reviewing the krouse flat cantilever specimen design [3],[4], see in the Fig.2.2 below for the proposed specimen design to test on the prototype.

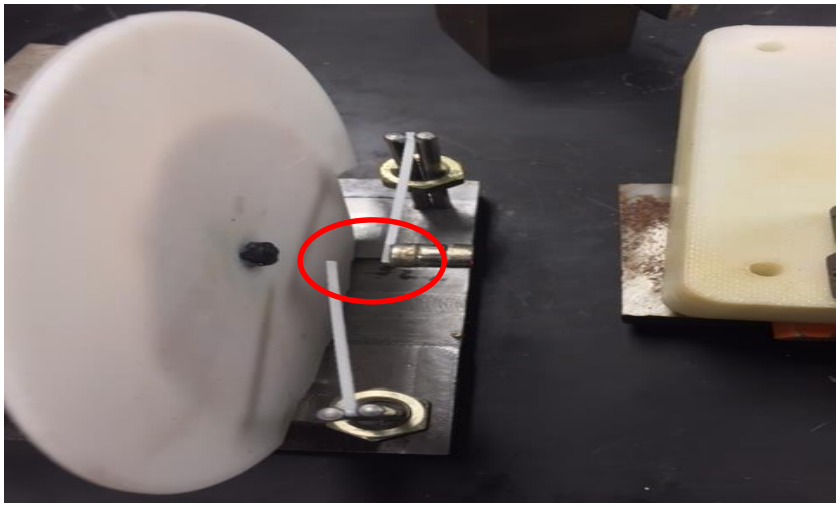

Figure 2.1 Flat specimen failing at the edge of the glued magnet

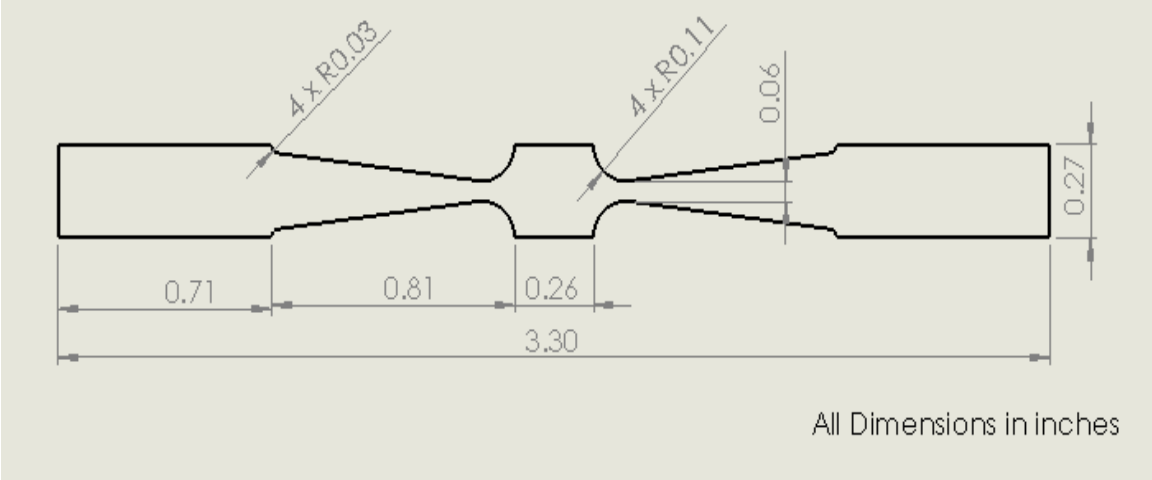


Figure 2.2 Final specimen design and the dimensions are all in inches

As shown in the Fig.2.2 the beam has two stress concentration zones, these zones taper to the beam center where 0.11 in diameter neodymium magnet was glued. To avoid any surface modifications due to the glue used to stick the permanent magnet, enough tolerance was given. Firstly, Specimen profile is machined from 0.25 in Aluminum 6061-T6 rolled bars using Wire EDM, then the attained 0.25in specimen profile is sliced to 0.026 in thick. To remove burrs and any surface artifacts from machining, the obtained specimens were ground on sand papers of 120, 400 and 600 grit. Total 22 specimens were taken for testing on the prototype.

200 ft. Thick enameled copper wire wound coil will have lower resistance and more turns. Magnetic core rod, ferrite has higher magnetic permeability, is chosen as the core for wound coil. Using 20guage wire 2.75 in length and 2.75 in diameter sized solenoid is made. This solenoid has 1000turns with 363 turns/in producing 44mH inductance. 50V DC supply is used to power the solenoid.

A small Neodymium magnet, 0.11 in diameter was glued at the center of the specimen. This permanent magnet glued to the specimen will take the magnetic impulses and causes displacement to the beam. Distance between the magnets greatly influences the magneto motive force between the magnets. Specimen with magnet was supported using the test setup close to the solenoid, placed less than 1cm between them. When the power

source was turned on, solenoid starts creating impulses, the faces of solenoid and magnet will have same polarity. As like poles repel, the magnet on the specimen is pushed away from the solenoid. This repelling force greatly depends on the current passing through the coil and distance between the magnets.

A simple-simple supported beam setup was prepared using a base plate and four dowel pins, as shown in the Fig.2.3 below [13],

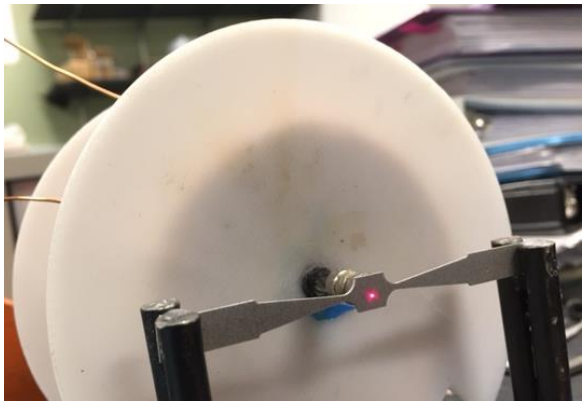

Figure 2.3 Simple-Simple supported test setup

## 2.2. ANALYSIS

A mosfet placed in series with the solenoid, was used as a switch. Arduino UNO, loaded with a program to turn on and turn off at required frequency. This generated the magnetic pulses from the solenoid. The pulses were usually set below 25 percent duty cycle, the frequencies were usually set near the resonant frequency of the specimen. Below Fig.2.4 shows the deflection caused due to individual impulses at non resonant frequencies. As known, every beam deflects with high amplitude when vibrated near resonant frequency, as shown in Fig.2.5 the displacements were amplified when the same strength impulse were given. Fatigue tests were usually performed with a specified constant R value, R, defined as the ratio of minimum strain/stress and maximum strain/stress. Particularly in this testing, R value was considered to be -1 i.e. fully reversed cycle. The magnitude of these deflections are recorded using laser displacement sensor, Keyence LK-H052, this sensor provided the amplitude of deflection with time.

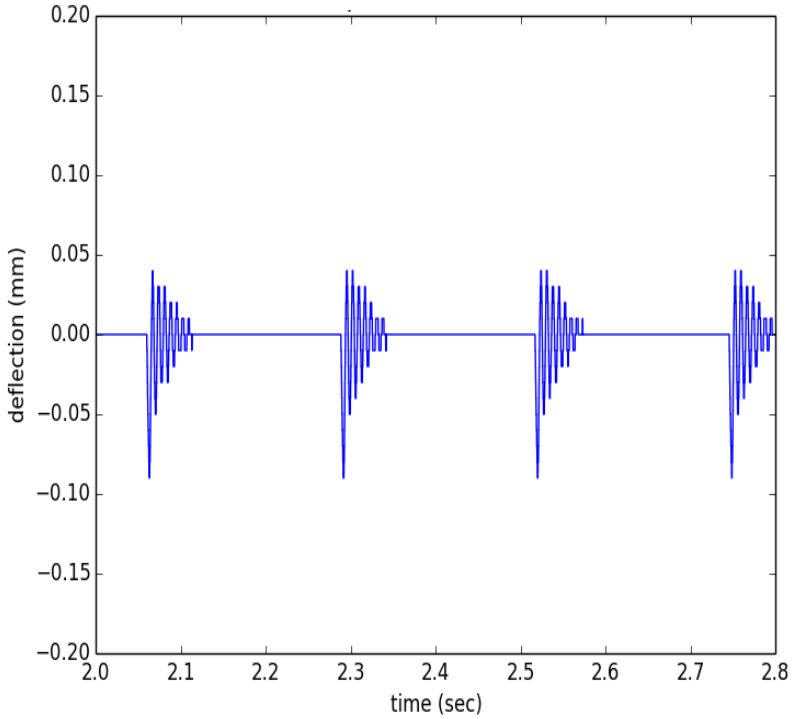


Figure 2.4 Deflections due to non-resonant impulses

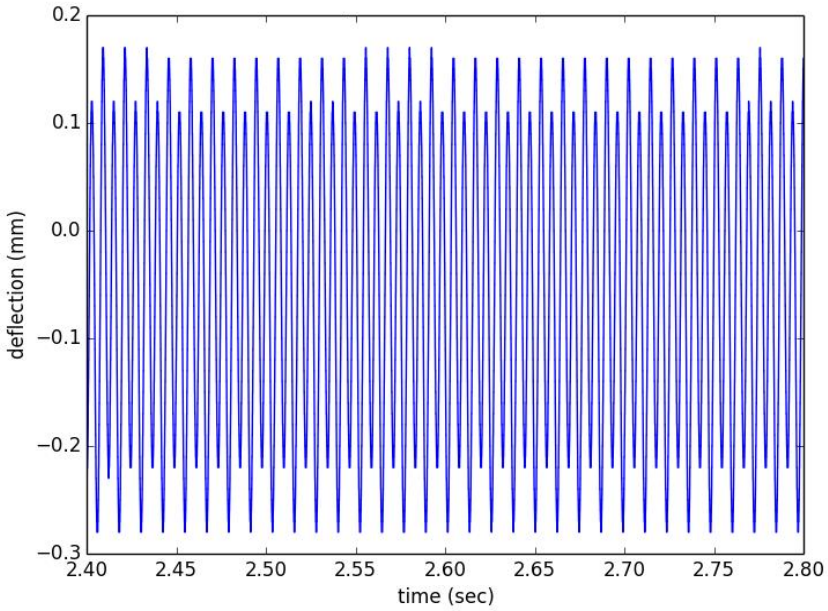


Figure 2.5 Deflections at neat resonant impulses

This way, cyclic strains as a sine wave with near resonant frequency were induced in the specimen. Applied deformation or amplitude of deformation was constant throughout the test. Finite element analysis had been performed on the designed specimen. The boundary conditions at the ends were simple-simple supported as discussed in the introduction part. Load field in the analysis was the forced displacement at the center of the beam and value of the displacement was the value recorded from the laser displacement sensor while testing. Figures 2.6, 2.7 and 2.8 below were results obtained from the finite element analysis. Figure 2.6 shows the deformation of the specimen stress profile, Fig.2.7 shows the closer look at the expected failure zones on the specimen, from Fig.2.7 it was evident that the neutral axis has zero stress when a beam was in purely bending. Figure 2.8a shows the compressive side and Figure 2.8b the tensile side when the specimen was bent.

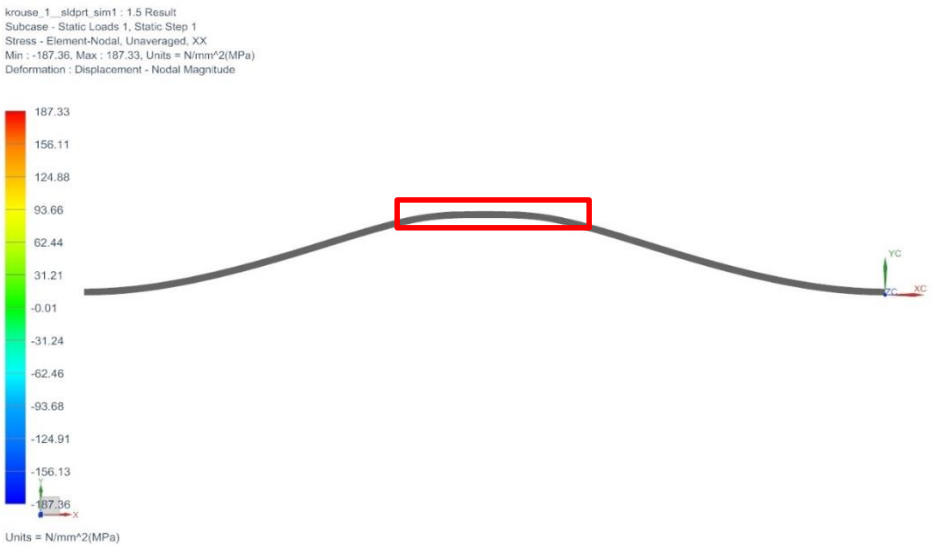


Figure 2.6 Deformation of a simple supported beam

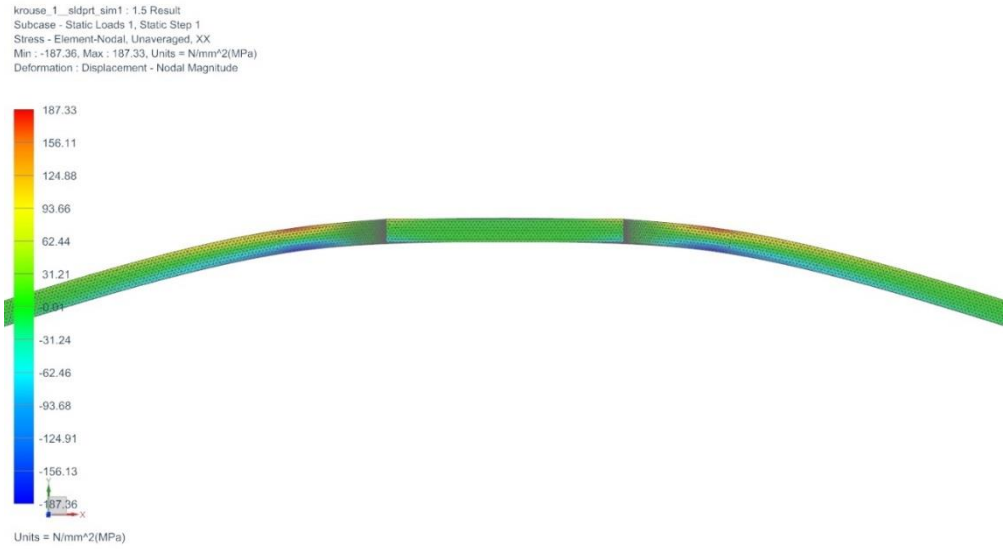


Figure 2.7 Stress from finite element analysis for 1.3mm (.051") deflection

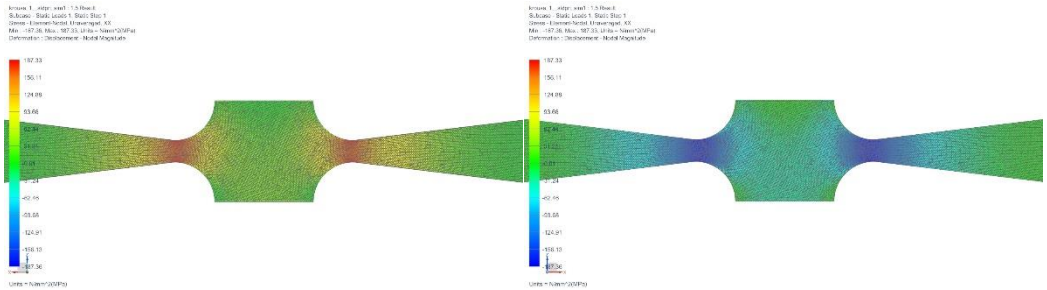

Figure 2.8 a) Maximum tensile stress side b) Maximum compressive stress side

Certain strains were selected and their respective displacements were induced in the specimen. These selected strain points were selected considering the capability of the 50V power supply in use. Initially 30V power supply was used, which comparably passes low current through the solenoid, this resulted in lower displacements and bending stresses induced in the specimen. Using 50V power supply increased the magnetic field strength of the solenoid resulting in higher displacements and bending stresses on the specimen. All the tests were performed vibrating the specimen from the maximum displacement achieved to the minimum displacement. Table 2.1 shows the strain points selected to test. The deflection amplitude mainly depends on current flow, distance between magnets and the thickness of the material.

Table 2.1 Calculation of respective strain and stress for selected deflections

| Deflection (mm) | Strain | Stress in MPa (ksi) |
|---|---|---|
| 1.5 | 9.6E-04 | 200.1 (29.0) |
| 1.34 | 8.6E-04 | 178.8 (25.9) |
| 1.25 | 8.0E-04 | 166.8 (24.2) |
| 1.2 | 7.7E-04 | 160.1 (23.2) |
| 1.1 | 7.1E-04 | 146.8 (21.3) |
| 1 | 6.4E-04 | 133.4 (19.3) |
| 0.9 | 5.8E-04 | 119.7 (17.4) |
| 0.8 | 5.1E-04 | 106.7 (15.5) |
| 0.7 | 4.5E-04 | 93.4 (13.5) |
| 0.5 | 3.2E-04 | 66.7 (9.7) |
| 0.45 | 2.9E-04 | 59.8 (8.7) |
| 0.35 | 2.2E-04 | 46.7 (6.8) |

In theory, after certain cycles, due to fatigue behavior, the specimen has to fail at the highest concentration zone. Using stop watch, the total time for the specimen to fail was recorded. Cycles to failure was calculated by multiplying the frequency of vibration to total time of the test.

## 3. RESULTS AND DISCUSSION

Total 27 specimens were prepared for testing on the prototype at R= -1, but only 12 specimens have successfully completed the test (fatigue failure) with R= -1 while other specimens have failed with different R values -0.5, -2 and -3. Figure 3.1 shows the fatigue failure of the specimen and Table 3.1 shows the stress, cycles and the reason for test termination at R= -1.

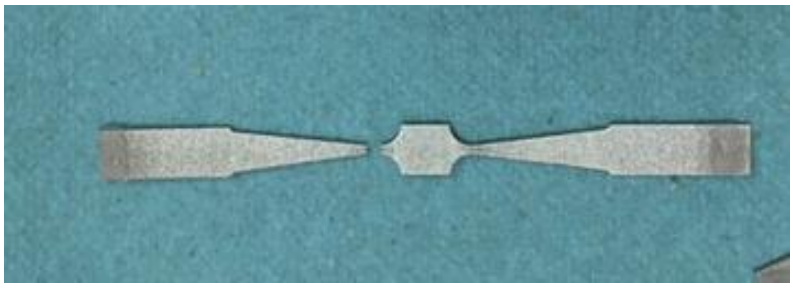

Figure 3.1 Fatigue failure of the specimen

Table 3.1 Fatigue test results

| STRESS in MPa (ksi) | CYCLES | RESULT |
|---|---|---|
| 200.16 (29.0) | 2.20E+05 | Failure |
| 178.81 (25.9) | 1.03E+05 | Failure |
| 166.8 (24.2) | 8.10E+05 | Failure |
| 160.13 (23.2) | 9.30E+04 | Failure |
| 151.7 (22.0) | 2.25E+05 | Failure |
| 146.8 (21.3) | 8.35E+05 | Failure |
| 133.4 (19.3) | 1.02E+06 | Failure |
| 119.7 (17.4) | 1.69E+06 | Failure |
| 106.75 (15.5) | 3.56E+06 | Failure |
| 93.41 (13.5) | 1.66E+07 | No Failure |
| 66.72 (9.7) | 1.19E+06 | No Failure |
| 59.89 (8.7) | 1.02E+07 | No Failure |

As per ASTM STP 91-A the S-N curve was plotted with specimens that have failed with fatigue at R= -1. S-N curve plot is made from the results obtained, see Fig.3.2,

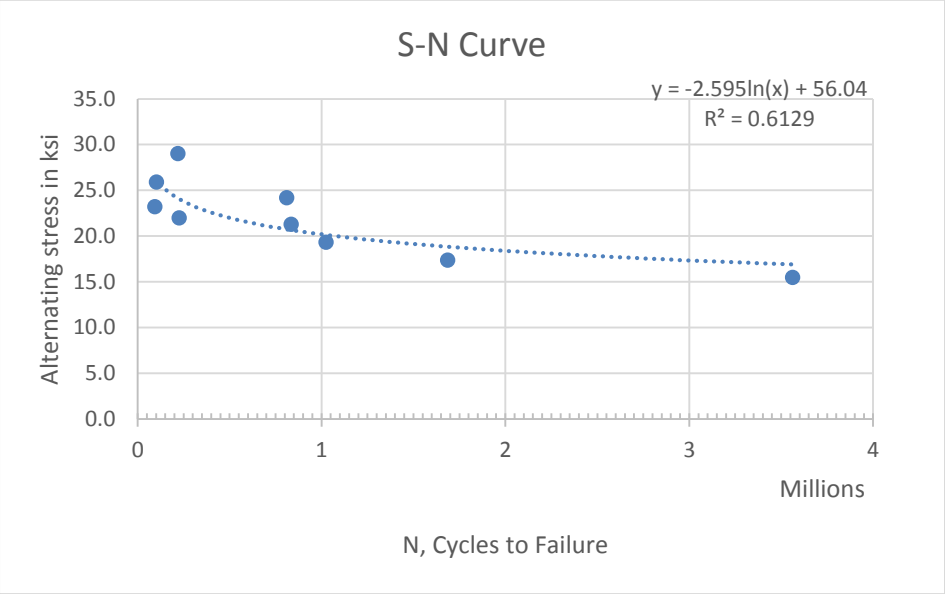


Figure 3.2 S-N curve for Aluminum 6061 T6

The probable reason low value for $R^2$ might be the inconsistency of supporting the specimen, preparation of the specimen and test speed. Though there were two probable failing zones, the specimen has failed randomly at either zones, this proved that the supports have been setup rightly as simple-simple beam and not biased on one side to failure. The test speeds were at the near resonant frequencies of the specimen, but the test speed was largely varied from 100 to 200Hz mainly due to the employed way of acquiring specimens. From the regression analysis, it can be concluded that the test setup is rigid but the specimen preparation had to be standardized. Below, the results are presented.

Product Form:

Grade designation: Aluminum 6061

Heat number: T6 Form of product: AMS 4117 $^1/_4$" thick bar

Last mechanical and thermal treatment: Hot –rolled and air cooled

Properties:

Tensile strength: 42 ksi

Yield strength: 35 ksi

Temperature: Room Temperature

Specimen Details: Unnotched and machined using wire EDM

Test Parameters

Loading: Bending

Frequency: 100Hz – 200Hz

Environment: Air

Regression analysis performed on all 12 specimen tested successfully, and equivalent stress equation is,

$$\sigma = -2.595 \ln(N) + 56.04$$

Aluminum does not exhibit knee in the S-N curve, so the infinite life was taken at 5 million cycles. Endurance limit at 5 million cycles for the tested material can be calculated from the equivalent stress equation obtained above and the value calculated was 16 ksi. Evaluating the proposed specimens design and machining and the loading type, the following correction factors [14] were considered: Size factor, $C_s$ varies with size and was more significant in reversed bending. For the specimen, designed thickness and breadth had size factor value 0.72. Surface finish factor, $C_f$ greatly varies with the process of acquiring the specimen i.e. machining or polishing. Mechanical properties always depend on the quality of surface finish of the specimen. Here, $C_f$ was 0.87 as the specimen are just machined using Wire EDM. Load factor, $C_l$ and temperature factor $C_t$ were equal to 1 because the load was reversed bending and test performed at room temperature.

The correction factors evaluated above are multiplied to the calculated endurance limit from the experiments to get a modified endurance limit ${S^1}_e$,

$${S^1}_e = C_s \times C_f \times C_t \times C_l \times S_e \times C_c \quad (38)$$

$${S^1}_e = 0.87 \times 0.72 \times 1 \times 1 \times 12 \times 1.51 \quad (39)$$

The modified endurance strength was calculated to be 15 ksi. Figure 3.3, from [15],[16] shows the S-N curve for Aluminum 6061 for different R values, experimental endurance strength of aluminum 6061 for 5 million cycles was marked on figure 3.3. The endurance

strength obtained from the prototype machine and the ASTM standard results were close enough.

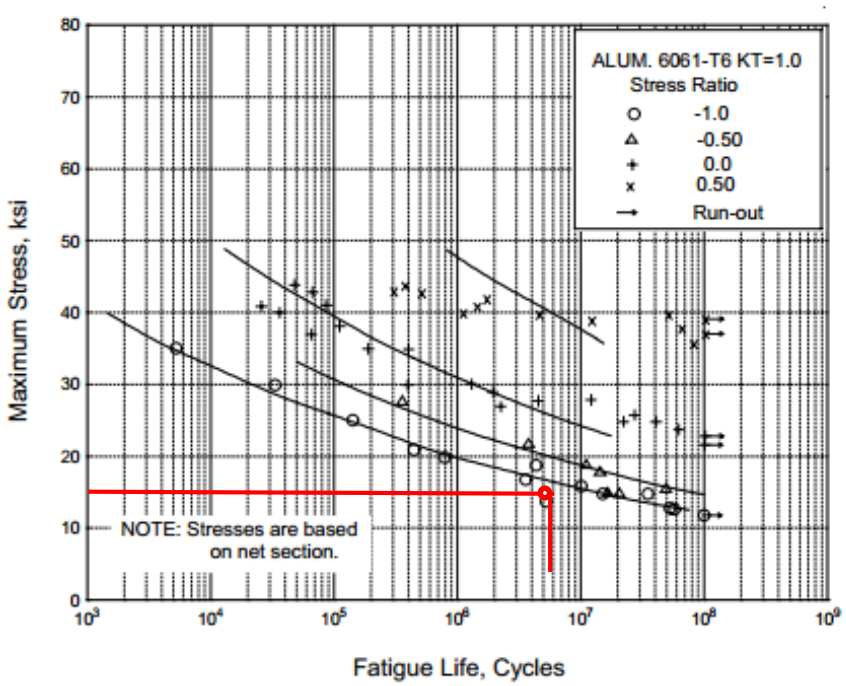


Figure 3.3 S-N curve for Aluminum 6061 T6

Hence, the concept of using magnetic impulses to induce bending stresses and fail the specimen with fatigue has been successfully proved.

# 4. CONCLUSION

The main objective of the current work was to model a working prototype which fastens the fatigue testing. Designed a prototype to test the fatigue life of any material which runs at near resonant frequency. The proposed design had no moving or touching parts, preventing the wear and failure of the test setup. Firstly, validated mathematical model of the Euler- Bernoulli beam to attain the strain and stress from its deflection amplitude was obtained. Secondly, designed the components required to build the machine prototype. Finally, a low strength material was chosen to test using the prototype. Prototype built was low force and high cycle machine, the speed of the test depended on the frequency of the specimen. All the prepared specimens were tested with the prototype and noticed that a million cycles could be achieved in 1.5 hours. Almost all the tests were performed at 100Hz to 200Hz, and this variation in frequency was mainly due to the change in thickness and inconsistency of supports. Experimental results, obtained with the prototype prove that the calculated endurance strength using this machine were comparable to the ASTM results. This principle can be used to fatigue test the variation in performance of a material of different alloys.

## 4.1. FUTURE WORK:

The test equipment had to be more standardized and automated. Specimen supports had to be more rigid to increase the repeatability of the testing. Using stroboscope can help determining the frequency of the specimen and adjust the forcing frequency to near resonant frequency [17]. When a fatigue crack develops, the natural frequency was reduced and the amplitude changes, constant displacement-type machines were equipped with automatic devices to detect and correct any change in deformation. Sometimes strain conditions imposed on the specimen were adjusted and kept under more or less close observation which can be possible by reading the laser displacement sensor and automatically adjust the pulse duration and frequency. More materials should be tested to confirm the results with ASTM.

## BIBLIOGRAPHY


[1] Gere, J. M., Timoshenko, S. P., "Mechanics of Materials," 4th ed. Boston: PWS Publishing Company, 1997.

[2] J. Schijve,"Fatigue of Structures and Materials," CBS Publishers, New Delhi, India 2009.

[3] Bulletins 46B and 46W, Krouse Testing Machine Co., Columbus, Ohio.

[4] Committee E-9 on Fatigue, "Manual on Fatigue Testing," American Society for Testing Materials, 1916 Race St., Philadelphia, USA.

[5] W. Nowacki, "Dynamics of Elastic Systems," John Wiley, New York, 1963.

[6] Voltera, Zachmanoglou, "Dynamics of Vibrations," Columbus, Charles E. Merrill Books, Inc., 1965.

[7] Coşkun Safa Bozkurt, Atay Mehmet Tarik and Öztürk Baki (2011), "Transverse Vibration Analysis of Euler Bernoulli Beams Using Analytical Approximate Techniques, Advances in Vibration Analysis Research," Dr.Farzad Ebrahimi (Ed.), ISBN: 978-953-307-209-8.

[8] Young, D., and R. P. Felgar, "Tables of Characteristic Functions Representing Normal Modes of Vibration of a Beam," Univ. Texas Bur. Eng. Research Bull. 44, July 1, 1949.

[9] Hoskins R. F., "Delta Functions: Introduction to Generalised Functions," Elsevier Science, March 2004.

[10] Bera, R.K., Bandyopadhyay, A.K., Ray, P.C., "Mathematical Physics for Engineers," Kent: New Academic Science Dec. 2008.

[11] Colakoglu, M., Jerina, K.L. (2003), "Material damping in 6061-T6511 Aluminium to assess fatigue damage Structures," vol. 26, no. 1, p. 79-84, DOI:10.1046/j.1460-2695.2003.00603.x.

[12] Robertson Will, Cazzolato Ben, and Zander Anthony, "Axial force between a thick coil and a cylindrical permanent magnet: Optimizing the Geometry of an Electromagnetic Actuator," School of Mechanical Engineering, The University of Adelaide, Australia.

[13] Fisher W. A. P. and Winkworth W. J., "The Effect of Tight Clamping on the Fatigue Strength of the Joints," Aeronautical Research Council Reports and Memoranda, Ministry of Supply, 1952.

[14] Hanson Michael D., "Fatigue Testing Techniques for Evaluating the Effects of Environment on Composite Materials," Army Air Mobility Research and Development Laboratory, Fort Eustis, Virginia, Oct 1974.

[15] Military handbook, "Metallic Materials and Elements for Aerospace Vehicle Structures," MIL-HDBK-5H, Decemeber 1998.

[16] Sanders W., "Fatigue Behavior of Aluminum Alloy Weldments," *Fatigue of Aluminum* Weld Res. Council Bulletin 171, 1972, pp.1-30.

[17] Wittenberghe Jeroen Van, Baets Patrick De, Wim De Waele, Wouter Ost, Matthias Verstraete and Stijn Hertelé , "Resonant Bending Fatigue Test Setup for Pipes with Optical Displacement Measuring System," ASME, 2012.

# VITA

Sai Aravind Palepu, was born on August 17 1990 and brought up in Hyderabad, India. He obtained his undergraduate degree in Mechanical Engineering from GITAM University, Visakhapatnam, India. During his senior year, he worked on project titled "Performance evaluation of lubricants dispersed with WS2 nano particles", under the supervision of Dr. V. Srinivas. His work involved dispersion of nano particles in conventional lubricant oil and evaluating the tribological properties of the oil. After his graduation, in spring 2013 he started pursuing master's degree in Manufacturing Engineering at Missouri University of Science and Technology, Rolla, Missouri.

During his course of study, he researched the potential of laser weld repair against TIG weld repair of Ti6Al4V machining defects. He received his M.S. degree in Manufacturing Engineering from Missouri University of Science and Technology in May, 2015.